ANALYSIS OF ALTERNATING CURRENT CIRCUITS

P. GODKHINDI
Editor, Circuit Specialist
C. LIN
Data Analyst, Circuit Specialist
K. THOMAS
Editor, Notebook Writer
N. VADIVELU
Data Analyst, MATLAB Specialist

(Received by 22 December 2016)

Five circuits were wired and connected to an alternating power source: an RC, RLC, transformer, and two solenoid circuits. A 24 Ω resistor and 100 μF capacitor created an RC circuit with a -(61.02±.03)° phase shift. A resonance frequency of (76±2) Hz was found in the RLC circuit. A transformer of 300 and 1200 winding coils yielded the greatest potential amplification, (4.95±.07), at a frequency of (583.0±.5) Hz. The magnetic field produced by both the disturbed and undisturbed Helmholtz coils matched the theory and a simulation, with an average signal-to-error ratio of 814.2 and 157.8 respectively.

I INTRODUCTION

Alternating current (AC) has numerous applications, especially when used alongside capacitors, inductors, transformers, and solenoids. An understanding of these four components and alternating current is a necessity.

II THEORY

The theory for the RC circuit was based upon the work of Godkhindi et al in Transients and Semi Conductors (2016).

In a circuit with AC power, the reactance of the capacitor is given by:

$$X_C = \frac{1}{2\pi f C} \quad [1]$$

(Hyperphysics, 2016)

Where:

X_C = reactance of capacitor (Ω)
f = frequency (Hz)
C = capacitance (F)

The beginning and ending potentials of a transformer are related by:

$$V_S = (V_P)\frac{n_S}{n_P} \quad [2]$$

(Hyperphysics, 2016)

Where:

V_S = potential of secondary coil (V)
V_P = potential of primary coil (V)
n_S = number of windings of secondary coil
n_P = number of windings of primary coil

In an RC circuit with AC, the phase shift between the potential and current waveforms is:

$$\phi = \arctan(\frac{X_C}{R}) \quad [3]$$

(Hyperphysics, 2016)

Where:

V = electric potential difference (V)
ϕ = phase shift (rad)
R = resistance of resistor (Ω)

The magnitude of the impedance of an RC circuit may be calculated using:

$$|Z| = \sqrt{R^2 + (X_L - X_C)^2} \quad [4]$$

(Hyperphysics, 2016)

Where:

$|Z|$ = impedance (Ω)

The resonance, or natural, frequency of the RCL circuit, was found with:

$$f_R = \frac{1}{2\pi\sqrt{LC}} \quad [5]$$

(McHutchon, 2013)

Where:

f_R = resonance frequency (Hz)
L = inductance (H)

The Biot-Savart Law describes the differential magnetic field of a point with respect to a differential point on a wire:

$$d\vec{B} = \frac{\mu_0 i d\vec{L}\times\vec{r}}{4\pi r^3} \quad [6]$$

(Halliday, 2011)

Where:

$d\vec{B}$ = magnetic field from one point (T)
μ_0 = permeability of free space (T m A^{-1})
i = coil current (A)
$d\vec{L}$ = infinitesimal length of conductor (m)
$\vec{r}$ = vector from current position to $d\vec{L}$

From [6], the on axis magnetic field of a solenoid is described as:

$$B(x) = \frac{\mu_0 i R^2}{2(R^2+x^2)^{1.5}} \quad [7]$$

(Halliday, 2011)

Where:

B = magnetic field (T)
R = radius of loop (m)
n = number of windings of wire
x = distance of point from the centre (m)

Vacuum permeability is defined as:

$$\mu_0 = 4\pi \text{ x } 10^7 \text{ T m A}^{-1}$$

(Halliday, 2011)

Uncertainty calculations and conventions were followed as outlined by van Bemmel (2016).

III Method

The BK Precision 4011A 5 MHz function generator output an AC into a circuit with an impedance of 50 Ω. Circuits requiring the function generator were designed to match this impedance.

In the RC circuit, a 100 μF capacitor and 24 Ω resistor were connected in series with the function generator, providing current at 36 Hz. The resistor and capacitor used in the experiment by Godkhindi et al (2016) could not be used because the reactance of a 10 μF capacitor was so great that no reasonable frequency could be used to obtain a 50 Ω impedance. Furthermore, the unreasonably high frequency calculated with the old components would result in a phase shift of roughly 0.004°, a value indistinguishable from equipment error. One voltmeter measured the potential of the entire circuit, and another the potential of the resistor. The potential of the capacitor was not directly measured to avoid erroneous readings near full charge. The voltmeters and LabQuests were found reliable by Godkhindi et al (2016).

In the RCL circuit, a 1.5 mF capacitor, four 100 Ω resistors in parallel, and a 2 mH inductor were connected in series with the function generator. Again, components from the prior experiment were changed to accommodate for impedance matching at a reasonable frequency. The resonant frequency was found to be (92.9±.3) Hz using [5] and [4]; here, the impedance of the circuit matched that of the function generator.

The voltmeter was set up across the resistors to measure potential in the circuit at various frequencies. Frequencies between 4.8 Hz and 225.6 Hz were tested at increments of approximately 20 Hz, with progressively smaller increments used closer to the resonance frequency.

Two 2 mH coils with 300 and 1200 windings respectively were paired with iron cores to create a transformer. The first coil was connected in series with the function generator and in parallel with the digital oscilloscope. The second coil was connected to the digital oscilloscope only. The potentials of the power source and both coils were recorded at various frequencies, ranging from 20 Hz to 1070 Hz in approximately 70 Hz increments.

To measure the magnetic field of a solenoid, two Helmholtz coils of radius (6.70±.01) cm were placed parallel 6.7 cm apart. The two coils, an ammeter, and the BK Precision 1506 40-watt power supply were connected in series. A ruler was centered through the two coils using textbooks and a level tool. The ruler was used to position the Vernier Magnetic Field Sensor along the longitudinal axis. To mitigate noise, 20 samples were collected per second and averaged over 10 seconds. The sensor itself was verified by measuring the B field of bar magnets and ensuring that the field strength decreased proportionally to the inverse square of the distance to the magnet. The values produced were compared with several other sensors to ensure the sensors accuracy.

The simulation was verified using the Helmholtz coils and a third proximate coil touching and forming a 60° angle with the second coil. A coordinate system was established with its origin at the centre of the two Helmholtz coils and the z-axis running through the centres of both coils and the y-axis vertical. A line 45° off the x-axis, was drawn on the lab counter, and then all three components of the verification measurements were taken along this line to maximize precision. The components were verified to be linearly independent through the use of a protractor.

IV Data

The solenoid simulation was verified by measuring the field of the set up in real life.

(x, z) Position (±0.02 cm)	Simulated Field (mT)	Measured Field (±0.0002mT)
(0, 0)	0.44774	0.5107
(3.54, 3.54)	1.55170	1.6306
(7.08, 7.08)	0.29768	0.3558
(10.62, 10.62)	0.15105	0.1902
(14.16, 14.16)	0.08367	0.0642

Fig. 1 - Simulated and Measured B-field of Helmholtz and Proximate Coils: The measured B field was the computed magnitude of the measured perpendicular components. The y position of the field was -(7.08±.02) cm.

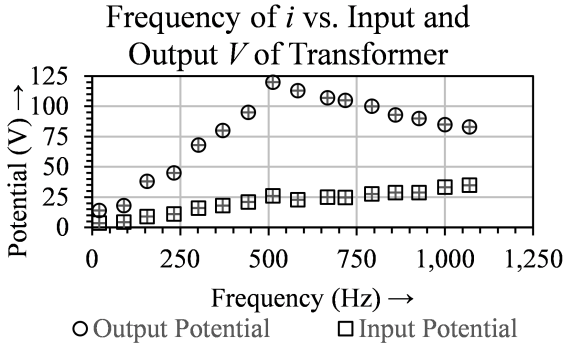

Fig. 2 - Frequency of Current vs. Input and Output Potentials of Transformer: The input and output potentials were graphed against the frequency. All points had an uncertainty of ±.1 V vertically.

V Analysis

Using Ohms Law, potentials across the resistors were divided by the resistance to obtain *i*. The potential of the entire circuit was plotted against the potential of the capacitor; the output replicated the Lissajous figure from the oscilloscope.

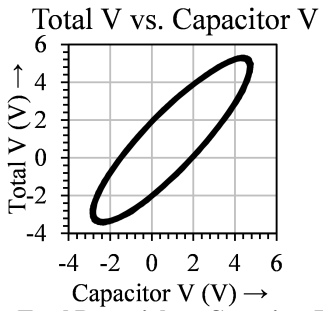

Fig. 3 - Total Potential vs. Capacitor Potetial: Due to the high number of data points in the Lissajous, a line plot was chosen to enhance clarity. All points had an uncertainty of ±.0005 V horizontally and vertically.

The ellipse was off-centre due to residual potential in the capacitor and wires. Analysis of the normalized figure yielded a phase shift of (59.89±.04)°.

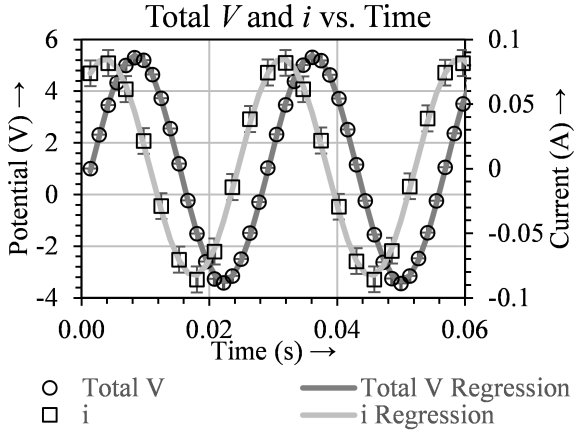

Fig. 4 - Total Potential and Current vs. Time: The circuit potential and current were both plotted against time. The phase shift between the two was too significant to be attributed to equipment error. Only two periods have been graphed for clarity.

The circuits potential and current wave forms were also plotted against time. The current was regressed to be:

$$i(t) = (0.0841 \pm .0002)\sin((226.60 \pm .01)t - (-1.065 \pm .002)) + (0.0013 \pm .0001) \quad [8]$$

Where:

i(t) = current at time t (A)

n = time elapsed (s)

The potential was regressed to be:

$$V_b(t) = (4.362 \pm .006)\sin((226.602 \pm .008)t) + (1.017 \pm .004) \quad [9]$$

Where:

V_b(t) = total potential (V)

The constants following each equation characterize the residual potential in the capacitor and wires.

The regressed angular velocities were used to obtain a frequency of (36.06±.01) Hz, which closely matched the frequency set by the function generator, 36 Hz.

Theoretical calculations predicted a phase shift of -61.504°, meaning that V_b should have lagged behind *i*. The horizontal translation in [10] was (-61.02±.03)°, confirming theory.

The phase shift obtained from the Lissajous was thought to be less accurate than that of the regression, because the Lissajous only considered the maxima of the produced

ellipse, whereas the regressions considered all the points.

The delay between i and V_b was caused by the capacitors reactance. A capacitor with a high capacitance requires less work to charge (and discharge), so it will not significantly resist an alternating current. This low work requirement explains why X_C is inversely proportional to capacitance. From [3], phase shift is also inversely proportional to capacitance. The 100 μF capacitor had a theoretical reactance of 44.209 Ω, while the regression showed a reactance of (43.33±.07) Ω; this supports the theory. The relatively high phase shift shows the difficulty in charging the capacitor.

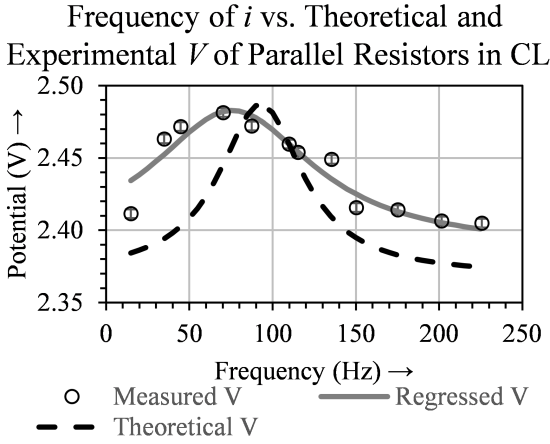

Fig. 5 - Frequency of Current vs. Theoretical and Experimental Potential Across Parallel Resistors in CLR Circuit: The potentials across the resistors were plotted against various frequencies, revealing a peak at (76±2) Hz.

A square reciprocal regression of resistor potential values against frequency yielded:

$$A_V(f) = \frac{(300\pm100)}{(f-(76\pm2))+(400\pm100)} + (2.39 \pm .01)\ [10]$$

Where:

A_V = potential function amplitude

f = frequency (Hz)

The square reciprocal relation was found by using the MATLAB non-linear fitting function. The reciprocal square relation was consistent with theory; impedance is quadratically related to frequency of current. Admittance is the reciprocal of impedance, and potential is directly related to admittance. Therefore, potential is related to frequency by the square reciprocal.

Using derivatives, a maximum value of (2.5±.2) V at (76±2) Hz was found. The predicted resonant frequency was 92.9 Hz.

The significant (18.2±.4)% discrepancy may have been due to the finite internal resistance of the voltmeter, or variances in the inductor's inductance and capacitor's capacitance, as the theoretical square reciprocal relation is contingent upon the circuit being impedance matched with the power source. This was likely the source of large uncertainties in [10] as well; any variances in capacitance or inductance would prevent the circuit from being impedance matched with the source, impacting the data.

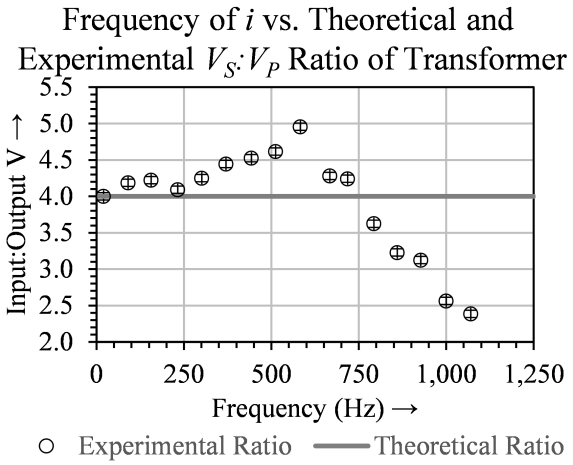

Fig. 6 - Frequency of Current vs. Theoretical and Experimental Potential Ratio of Transformer: The experimental ratios between the potentials were plotted at various frequencies, alongside the theoretical ratio of 4.0.

The highest amplification of potential was by a factor of (4.95±.07), and occurred at a frequency of (583.0±.5) Hz. This peak was present because transformers are designed to perform optimally at a certain frequency. According to [2], the expected ratio between potentials was 4:1. This was not the case, due to energy loss and variances in the used equipment.

The energy loss occurred for numerous reasons, including the resistance of the copper wire used in windings. Moreover, it was thought that some of the magnetic field lines formed were not strong enough to induce a current at sufficiently low frequencies. As a result, they collapsed. Hysteresis loss occurred when the field within the transformer was reversed too rapidly, resulting in thermal loss.

Induced due to the changing magnetic field, eddy currents occurred at higher frequencies. They were especially prominent

due to the high conductance of the iron core. The eddy currents resisted the current induced by the magnetic field, leading to heat loss. Thus, at adequately high frequencies, the spinning magnetic dipoles would not have been able to maintain their oscillation, and therefore could not induce a current.

Since [7] describes the on-axis magnetic field of one solenoid, the following expression was derived to model the on-axis magnetic field of the Helmholtz coils:

$$B_H(x) = B(x+\tfrac{R}{2}) + B(x-\tfrac{R}{2}) \qquad [11]$$

The measured magnetic field was plotted against the theoretical and simulated fields.

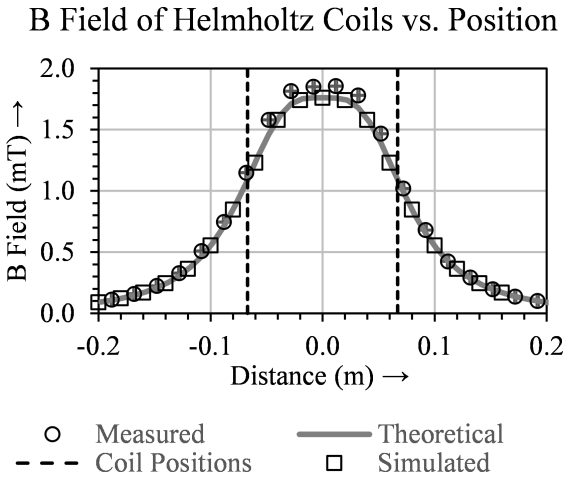

Fig. 7 - Measured, Theoretical, and Simulated B Field of Coil: The theoretical, simulated, and measured on-axis magnetic field of the coils of radius (6.70±.01) cm with (0.410±.001) A of current and 320 windings each.

The measured data conforms with the accepted theory. A mean-squared error (MSE) analysis was enacted on the data, which produced an MSE of 0.0034, and a signal-to-error ratio of 814.2, showing a strong correlation between the theoretical and measured values. The drop-off shown between the coils is due to the imperfect nature of the Helmholtz coils, as they cannot maintain a uniform field as effectively as a continuous solenoid. The difference in the peak values was (92±4) μT. The slight variation found at the peak of the curve was likely due to human error, as slight directional and positional misalignment would result in a higher field reading, as the field of a Helmholtz coil is greater in magnitude closer to the coils.

A simulation was written in MATLAB to model the solenoid circuit. This simulation was verified using the Helmholtz coils without (see Figure 7) and with (see Figure 1) the proximate coil. A mean square error analysis of the latter revealed an MSE of 0.003096, which resulted in a signal-to-error ratio of 157.8 between the measured and simulated values. This showed a strong correlation, which proved the simulation accurate.

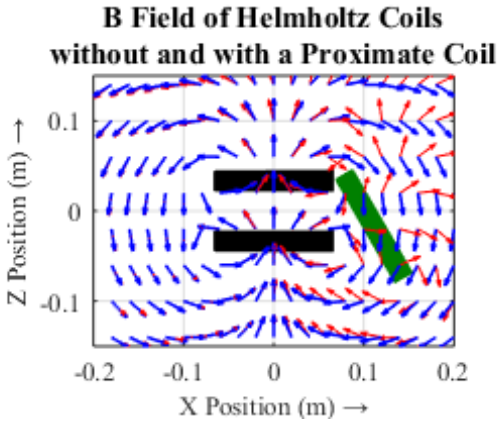

Fig. 8 - Vector Plot of B Field of Helmholtz Coils with and without Proximate Coil: The plot above shows the Helmholtz coils (black) as arranged in the experiment with a proximate coil (green) of the same physical properties. The blue vector field represents the undisturbed field while the red shows the disturbed field. Both fields were normalized then scaled for clarity.

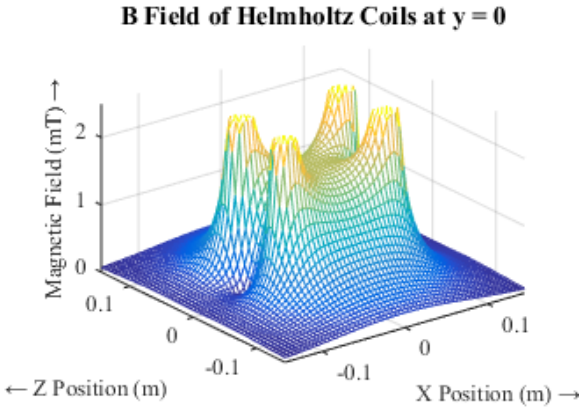

Fig. 9 - Magnetic Field of Helmholtz Coils The graph above shows the magnitude of the magnetic field with the Helmholtz coils parallel to the X axis. This plane corresponds to y = 0 on Figure 8. The graph was cropped at 2.5 mT for clarity, as the field close to the solenoids is significantly higher.

The symmetry observed in the magnitudes and directions of the magnetic fields around the Helmholtz coils matched theory.

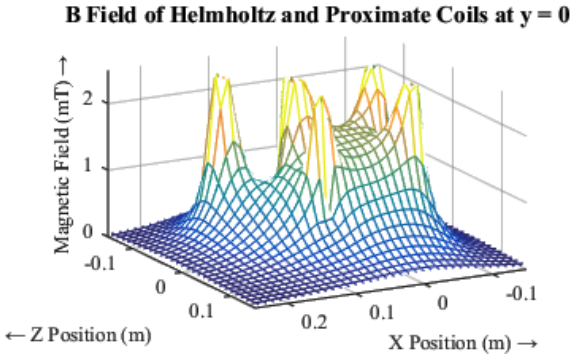

Fig. 10 -Magnetic Field of Helmholtz and Proximate Coils The graph above shows the magnitude of the magnetic field with the proximate coil with the Helmholtz coils parallel to the X axis. The graph was cropped at 2.5 mT for clarity, as the field close to the solenoids is significantly higher.

Comparing both the directions and magnitudes of the magnetic field from the Helmholtz coils alone to the coils with another proximate coil revealed significant differences, especially in the off-axis regions. The former displays the predicted symmetry, while the latter displays no such symmetry in the fields. Furthermore, the magnitude of the field after the third coil was introduced increased significantly, which matches theory.

VI Sources of Error

Because the wiring components used were not ideal, noise from residual potential in the components was inevitable. Furthermore, the capacitor and inductor created reactances that deviated from ideal theory. As a result, the two had unaccounted resistances, causing a disparity between the theoretical and measured values in the RC and RCL circuits.

The measurements of potential acquired with the voltmeter in the transformers circuit were not completely accurate, since the potential probe had residual finite resistance, impacting the measurements taken.

For the solenoid circuit, the most significant source of error stemmmed from sensors ability to only measure the magnetic field in one direction, meaning even the slightest variation in the angle of the probe would impair the accuracy of the measurements. This perturbation was minimized using the ruler and lab bench, but was inevitable nonetheless.

VII Conclusion

Through the analysis of the five AC circuits, properties of each circuit were concluded. The RC circuit yielded a phase shift of (-61.02±.03)° with a 24 Ω resistor, a 100 μF, and 36 Hz of alternating current.

The RCL circuit reached resonance at a frequency of (76±2) Hz, a (18.2±.4)% discrepancy from the predicted value of (91.88±.03) Hz.

The transformers yielded maximum amplification at a frequency of (583.0±.5) Hz, magnifying the potential by a factor of (4.95±.07). From here, the output potential began to drop off due to numerous forms of energy loss.

The solenoid circuits revealed a strong correlation between the theoretical and observed B fields, with an average signal-to-error ratio of 814.2, the greatest difference being just (92±4) μT at the centre.The simulation showed the symmetric properties of the magnetic fields of an undisturbed coil versus the asymmetric fields with a proximate coil.

VIII Sources

Godkhindi et al, DC Transients and Semi Conductors Analysis, 2016

Halliday & Resnick, Fundamentals of Physics 9th Ed, 2011

Hyperphysics, RC Circuit, 2016.

McHutchon, RLC Resonant Circuits, 2013

van Bemmel, H., Handling of Experimental Data, Marc Garneau C.I. Physics Dept., 2016